Fibers and Polymers 2015, Vol.16, No.12, 2617-2626
DOI 10.1007/s12221-015-5637-7

ISSN 1229-9197 (print version)
ISSN 1875-0052 (electronic version)

Enhanced Thermal Properties for Epoxy Composites with a Three-dimensional Graphene Oxide Filler

Jian Gao[1], Jinhong Yu[1,2]*, Xinfeng Wu[3], Baolin Rao[1], Laifu Song[1], Zihai He[1], and Shaorong Lu[1]*

[1]*Key Laboratory of New Processing Technology for Nonferrous Metals and Materials, Ministry of Education, School of Material Science and Engineering, Guilin University of Technology, Guilin 541004, China*
[2]*Key Laboratory of Marine Materials and Related Technologies, Ningbo Institute of Materials Technology and Engineering, Chinese Academy of Sciences, Ningbo 315201, China*
[3]*College of Ocean Science and Engineering, Shanghai Maritime University, Shanghai 200240, China*
(Received August 26, 2015; Revised October 18, 2015; Accepted November 19, 2015)

Abstract: In this study, we report a simple and efficient method to prepare three-dimensional graphene oxide (3DGO) network by freeze drying and investigate the effect of 3DGO network on thermal properties of epoxy composites. It was found that the 3DGO network not only improved thermal conductivity, thermal stability, glass transition temperature and storage modulus of epoxy composites, but also reduced the thermal expansion properties of epoxy composites. For instance, the thermal conductivity value of epoxy composite with only 1.3 wt% 3DGO is 0.62 $Wm^{-1}K^{-1}$, increased by 148 % in comparison with that of the neat epoxy (0.25 $Wm^{-1}K^{-1}$).

Keywords: Epoxy, Three-dimensional graphene oxide, Thermal conductivity

Introduction

Epoxy resin, as a very important thermosetting polymer, have been widely employed in many field such as electronic equipment materials, coating and adhesives [1-4], aerospace industry materials [5] due to its outstanding properties of physical and chemical stability. However, with the rapid development of electronic integration technology, electronic components become more and more miniaturization and functionality and the logic circuits tend to be complex [6,7]. In the high frequency working environment, electronic components will quickly produce a lot of heat, and a lot of heat accumulation would evidently reduce the life and reliability of electronic components because of softening or inflation of electronic components [8]. Therefore, it is crucial to improve the heat-resistant properties and thermal conductivity of electronic materials. The use of conventional epoxy resins, with low thermal conductivity (0.2 $Wm^{-1}K^{-1}$), are not satisfy with the quick dissipation of heat from electronic device [9]. So far, research works on improving thermal conductivity of epoxy resins has caused wide concern over the recent years.

Many efforts to achieving high thermal conductivity of epoxy composites were reported. Cementation is a general method in the high-integrated electronic capsulation with high thermal conductive adhesives [10]. The traditional high thermal conductive composites are manufactured by filling high thermal conductivities fillers into polymer matrix. Metal particles exhibit unique properties because of the small sizes and high thermal conductive, such as Al [11], Cu [12], Ni [13], and Ag [14]. In addition, previous researches that inorganic compound fillers with high thermal conductivity are also used to increase the thermal conductivity of composites, such as Al_2O_3 [15], AlN [15], BN [16], etc. But the loading fraction of the fillers always exceed 30 wt%, which result in poor mechanical properties. Furthermore, it is very difficult to control the dispersibility of fillers in the polymer matrix [17,18].

Carbon, as based materials, and its various morphologies have been brought into the polymer matrix to improve thermal conductivity [19-22]. For example, the thermal conductivity values for single-walled carbon nanotube (SWNT) is 6000 $Wm^{-1}K^{-1}$ at room temperature [23]. Beside, monolayer graphene with a high thermal conductivity (about 5000 $Wm^{-1}K^{-1}$) has also been used to increase the thermal conductivity of epoxy resins [24,25]. Unfortunately, the large specific surface area and high cost of graphene led to the decrease of doping concentration [26,27].

In this study, we report a rapid and simple strategy for the preparation of three-dimensional graphene oxide (3DGO). Three dimensional structure graphene oxide were obtained by employing the freeze drying process. Subsequently, the 3DGO fillers were poured into the epoxy matrix to enhance its thermal properties. The thermal properties of the epoxy composites were systematically investigated. The results demonstrated that the 3DGO fillers can effectively enhance the thermal conductivity of the epoxy composite due to the formation of 3D interconnected network structure with significantly reduced thermal interface resistances.

Experimental

Materials

3,4-epoxycyclohexylmethy-(3′,4′-epoxy) cyclohexane carboxylate (UVR6105) was provided by DOW Chemical

*Corresponding author: yujinhong@nimte.ac.cn
*Corresponding author: lushaor@163.com

(USA); Methyl-hexahydrophthalic anhydride (MHHPA) was obtained from Shanghai Li Yi Science & Technology Development Co., Ltd. (China); Neodymium (III) acetylacetonate ($Nd(acac)_3$) used as latentcatalyst was purchased from Aldrich Chemicals. Nature flake graphite with the size of 325 mesh was provided by Hengrui Graphite Co., Ltd. (China); H_2O_2 (30 %), $KMnO_4$, H_2SO_4 (98 %), HCl (36 %), P_2O_5 and $K_2S_2O_8$ were purchased from Sinopharm Chemical Reagent Co., Ltd. (China).

Preparation of Graphene Oxide (GO)

GO were prepared through oxidization of nature flake graphite by modified Hummers method [28-31]. In the preoxidation step, 80 m*l* H_2SO_4 (98 %) was put into a 800 m*l* round-bottom beaker placed in water bath, $K_2S_2O_8$ (10 g) and P_2O_5 (10 g) were dissolved in H_2SO_4 at 90 °C under stirring. After the mixture were completely dissolved, adding (3 g) Graphite powder slowly, and the solution was kept at 90 °C for 4.5 h under intensive stirring. Then the solution was cooled to room temperature, washed and filtered to remove the residual acid with a large amount of deionized (DI) water. The product was dried at 60 °C overnight.

In the second oxidation step, the pretreated product was introduced into a 800 m*l* round-bottom beaker loaded with 150 m*l* H_2SO_4 (98 %) under the condition of ice water bath. Then $KMnO_4$ (10 g) was added slowly to the above H_2SO_4 solution, and the temperature of the solution was kept below 10 °C until $KMnO_4$ was added completely. After that, the system was heat to 35 °C and reacted for 2 h. Then 600 m*l* DI water added dropwise to the solution under room temperature and stired sequentially for 7 h. 30 % H_2O_2 was poured into mixture until the color of the mixture changed to brilliant yellow, indicating a high oxidation level of graphite. The mixture then washed with HCl and DI water by centrifuging several times. The remaining solid material was dispersed in DI water and ultrasounded for 0.5 h. Finally, the suspension was centrifuged at the speed of 12000 rm, and taking the upper brownish suspension to obtain the high quality GO.

Preparation of 3DGO/epoxy Composites

The epoxy composites were prepared as follows: Firstly, the brownish GO suspension was concentrated by rotary evaporation for 0.5, 1, 2 h to obtained different concentration of GO suspension. Then concentration of GO suspension (20 m*l*) was poured into diameter of 60 mm glass culture vessel and sealed by film with many small holes through them. After that, the glass culture vessel containing the GO suspension was put in refrigerator for 12 h to freeze to the ice. Finally, the glass culture vessel was transferred to freezing and drying machine, drying for 24 h, removing water by the form of ice sublimation to get 3DGO. Secondly, $Nd(acac)_3$ was added to the epoxy resin and stirred until completely dissolved at 80 °C in a beaker. After that, MHHPA was added under vigorous stirred for 30 min and then the solution was cooled down to the room temperature. The mass ratio of epoxy, MHHPA and $Nd(acac)_3$ is 100:95:0.5. Finally, the solution of epoxy/MHHPA/$Nd(acac)_3$ was injected into the 3DGO, pre-cured in an oven at 135 °C for 2 h and post-cured at 160 °C for 14 h. the experimental details of the process of preparation is shown in Figure 1.

Characterization

Fourier-transform infrared spectra (FT-IR) were recorded

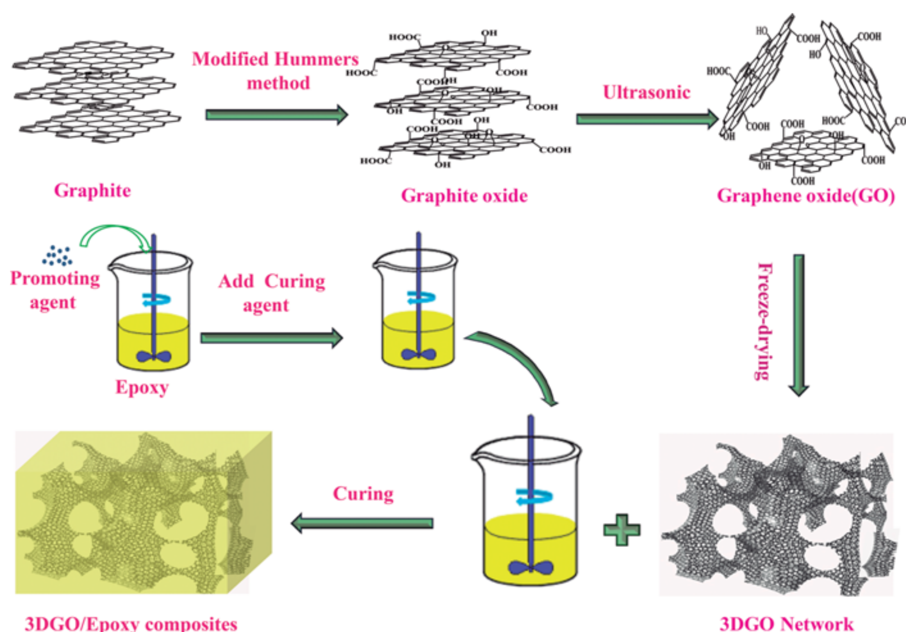

Figure 1. The preparation process of epoxy composites.

on a Nicolet Nexus 470 (FT-IR, Nicolet Nexus 470, USA) over the range of 4000-400 cm^{-1}. Raman spectra was excited DXR Raman Microscope (Thermo Fisher Scientific DXR, Thermo Electron, USA) with a laser of 532 nm. X-ray Photoelectron Spectroscopy (ESCALAB 250Xi, Thermo Scientific, USA) were recorded at 30 eV pass energy, 0.5 eV/step, using a specs spectrometer, equipped with a dual-anode X-ray source Al/Mg, energy analyzer and a multi-channel detector. AFM images were obtained using a Scanning Probe Microscope (Ntegra Prima SPM, NT-MDT, Russia), and the samples for AFM measurement was prepared by GO aqueous suspension onto an atomically smooth synthetic mica support. The morphology of samples was observed by utilizing a field emission scanning electron microscope (FE-SEM, JSM-6701F, Japan) at an accelerating voltage of 20 kV and the fracture surfaces was sputtered with thin layers of gold to improve the conductivity. Thermal stability of the specimens was measured by using TGA Q-500 thermogravimetric analyzer (TA Instruments, USA), and the test temperature was from room temperature to 500 °C at a heating rate of 10 °C/min under N_2 protection.

Thermal conductivities of the composites were measured with LFA 447 Nanoflash apparatus (NETZSCH, Germany) at room temperature. The samples were prepared in round shape with the diameter of 6 mm and the thickness of 1 mm. Thermal infrared images on neat epoxy and its composites were taken by thermo tracer TH6200 (NEC, Japan). Dynamic mechanical analysis (DMA) was conducted on a DMA Q-800 dynamic mechanical analyzer (TA Instruments, USA) in the single cantilever mode with Single-frequency patterns and multi-frequency patterns. The test of Single-frequency patterns was performed with a frequency of 1 Hz from 30 °C to 250 °C at the heating rate of 3 °C/min. For multi-frequency patterns, the test was arranged from 30 °C to 300 °C at a heating rate of 0.5 °C/min with 0.5, 1, 5, 10, and 15 Hz. Coefficient of thermal expansion of specimens was recorded on a thermal dilatometer (DIL 402C, NETZSCH, Germany) with the size of 25×2.5×2.5 mm at the heating rate of 3 °C/min from 20 °C to 160 °C.

Results and Discussion

Characterization of GO and 3DGO

Fourier-transform infrared spectra (FT-IR), Raman spectra and XPS spectrum of GO were shown in Figure 2. The FTIR spectra of NG and GO are presented in Figure 2(a). Clearly, A tiny band of hydroxyl group (-OH) at 3427 cm^{-1}, C-H band at 2924 cm^{-1} and C=C band at 1570 cm^{-1} were observed in NG spectrum. Compared to the spectra of NG, the hydroxyl group (-OH) has become a broad and intense band and transferred from 3427 cm^{-1} to 3438 cm^{-1} because of the effect of C=O, and C=O stretching at 1723 cm^{-1} are clearly

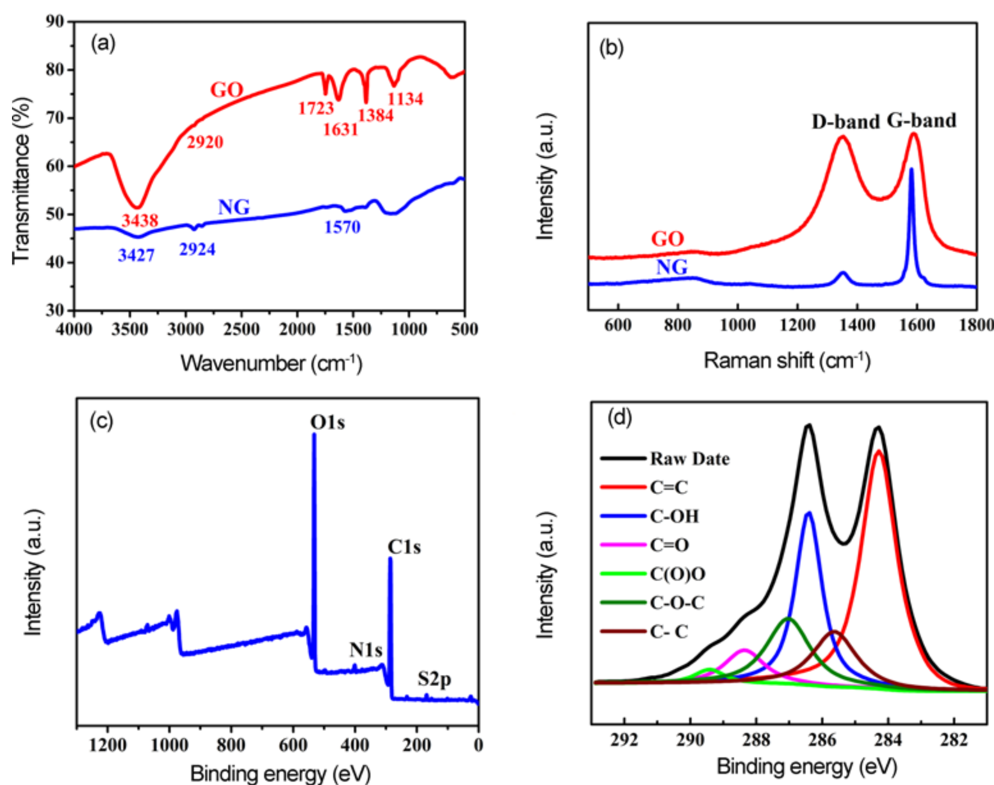

Figure 2. (a) FT-IR spectra of NG and GO, (b) raman spectra of NG and GO, (c) XPS survey spectra of GO, and (d) C1s XPS spectrum of GO.

observed from the spectra of GO, which come from carboxyl group (-COOH) on the edge of GO sheets. In addition, several new peaks such as C-OH stretching at 1384 $cm^{-1}$and C-O-C symmetric and asymmetric stretching vibration at 1134 cm^{-1} also appeared in GO spectra. These results indicated that the oxygen atom (O) was brought in during the GO synthesis process.

Raman analysis was applied to illustrate the orientation of layer and types of edge of the NG and GO samples in Figure 2(b). D bands, represented sp^3-hybridized carbon atoms [32], were located in 1353 cm^{-1} in the Raman spectra of NG and GO. Correspondingly, G bands represented sp^2-hybridized carbon atom, has shifted from 1581 cm^{-1} of NG to 1589 cm^{-1} of GO because of the decreasing thickness of the layers of GO. The intensity ratio of the D and G peaks (I_D/I_G), as an indicator of oxidation degree of graphite oxide [33], is about 0.99 in the spectra of GO, which is higher than that of NG (I_D/I_G=0.18). The increasing value of I_D/I_G indicated that the strong oxidation really damaged the NG and left a high defect during the preparation of GO [34]. These results suggested that the oxidation promoted the exfoliation of NG. The stronger was the oxidation, the more sheets of GO could be produced.

XPS analysis was employed to quantitatively elucidate the chemical nature of GO. Sulphur (S) was come under observation from the survey spectra of GO shown in Figure 2(c), located at binding energies (BE) of 168.6 eV, indicating that SO_4^{2-} was not removed completely. A lower C/O atomic ratio for GO was calculated as 2.9, indicate the successful modification of GO, which is further confirmed by the characteristic peaks of carbon-based atom functional groups shown in Figure 2(d). The deconvolution of XPS spectra is dominated by a very intense peak assigned to the C=C (sp^2 carbon framework), located at binding energies (BE) of 284.3 eV respectively. Beside this mainline, five other spectral features dependent on the chemical environment experienced by the carbon atoms could be observed and, as a result, can be assigned to different carbon containing groups. The deconvolution shows that at the edges of the sp^2 network structural disorder is found due to the carbon-hydrogen bonded groups in sp^3-hybridized state appear at 285.5 eV. In addition, functional groups are also present, such as C-O-C (287.1 eV), C=O (288.4 eV), C(O)O (289.5 eV), C-OH (286.3 eV), which the key factors toenable GO to be easily exfoliated in an aqueous solution. These results are consistent with other literature reported [35,36], and further confirm the above content stated in FT-IR and Raman analysis.

Figure 3(a) shows the AFM images of the exfoliated GO

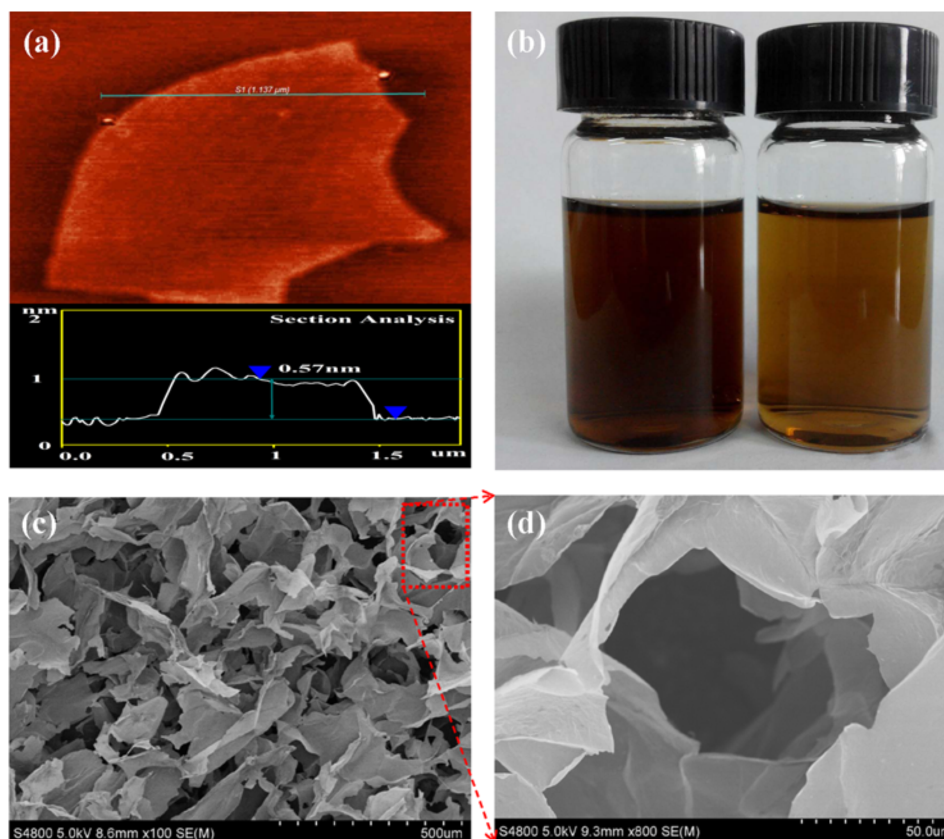

Figure 3. (a) AFM images of GO, (b) dispersion of GO in water (left: 0.5 mg/m*l*, right: 0.3 mg/m*l*), (c) low magnification, and (d) high magnification SEM images of 3DGO.

sheet. It is clearly to see the flake structure of GO and the thin thickness is about 0.57 nm, which is thicker than 0.34 nm of single layer structure of ideal GO. That is because the oxidation lead to the transformation of carbon atoms bonding from sp^2 to sp^3 and the bonding of oxygen groups around the flat sheet of carbon atoms, such as carboxyl, hydroxyl and epoxy groups [32]. It's worth noting that the thickness of the graphene in the edge is higher than the center, indicating that the oxide of graphite is from outside to inside and oxygen-containing functional group distributed mainly in the edge regions. Meanwhile, the undulating surface of GO resulted from nanometer effect, and topography can be also affected by residual solvent and mica surface roughness. Figure 3(b) shows the photographs of the different concentration GO aqueous solution. The GO was homogeneously dispersed in water by ample hydrophilic group (-COOH and -OH) distributed around the edge of GO. The SEM images of the 3DGO are shown in Figure 3(c) and (d). All of them present a foam-like structure with numerous interconnected pores, the size of the aperture is about several decades of micrometers and the pore walls was supported by GO sheets. According to unidirectional freezing, the growth of ice crystals compacts the GO sheets between the boundaries of adjacent crystals [37]. Moreover, when ice sublimes it turns directly into a gas from a solid bypassing the liquid state, which does not destroy the three-dimensional network structure but help the formation of this structure. In addition, hydrogen bonds between oxygen-containing functional groups of GO as well as π-π interactions have play a great role in the stability of the structure.

Morphology of Epoxy Composites

The morphologies of the fracture surfaces of the neat epoxy and its composites were recorded by SEM, as shown in Figure 4. The fracture surfaces of the neat epoxy is very smooth and similar to river patterns, indicating brittle fracture [38]. Relatively, the fracture surfaces of epoxy composites exhibit a rougher fracture surface with numerous gullies and wrinkle, especially the fracture surfaces of epoxy composites with 1.3 wt% 3DGO, suggesting that the fracture mechanism of epoxy composites was transformed to ductile fracture from brittle fracture with 3DGO. Moreover, the network GO are embedded in the epoxy matrix and do not separate themselves from the epoxy matrix. When micro-cracks encounter high-strength GO sheets, the fracture has to bypass them and seek alternative routes, and consequently, the GO sheets have pulled out from epoxy matrix and lead to the formation of wrinkled area. In contrast to brittle fracture, ductile fracture burn more energy in the breaking process, so the strength of the material has enhanced by participation of GO [39].

Thermal Properties of Epoxy Composites

Thermal stability of the cured epoxy resins was assessed by TGA under nitrogen atmospheres. Figure 5 shows the TGA and DTG curves of the neat epoxy and its composites.

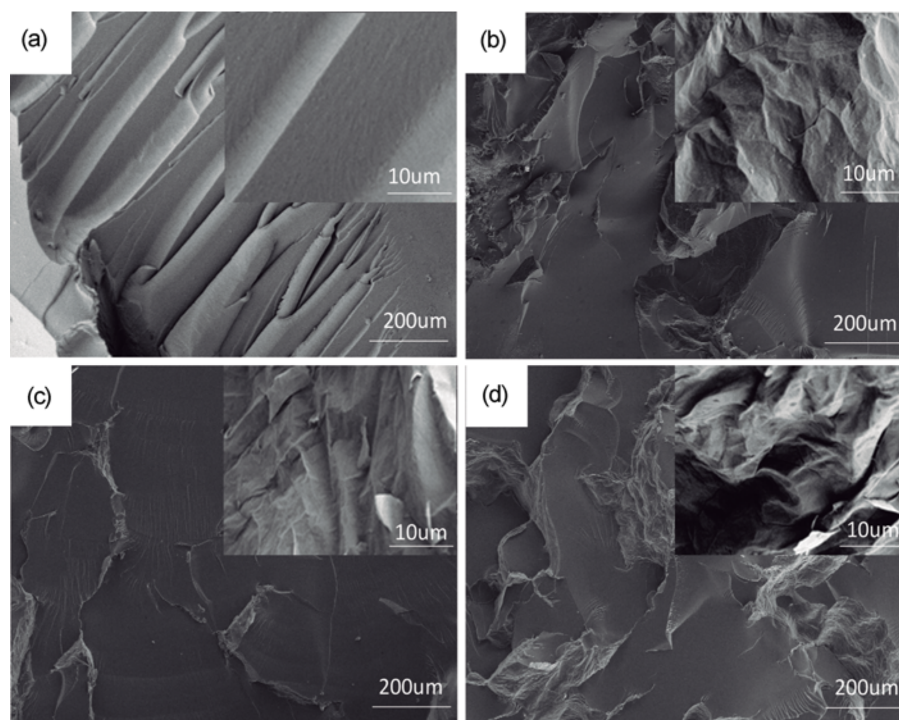

Figure 4. SEM images of: (a) neat epoxy, (b) 0.3 wt% 3DGO/epoxy composite, (c) 0.8 wt% 3DGO/epoxy composite, and (d) 1.3 wt% 3DGO/epoxy composite. Inset illustrates the high magnification images.

It is obviously seen that all curves of the specimens are very similar and only one-step decomposition, in other words, the introduction of 3DGO did not change degradation mechanism of the epoxy matrix. Simultaneously, a high thermal stability of 3DGO/epoxy composites was exhibited in Figure 5(a), the decomposition temperatures (T_d) of composite at 5 % weight loss took places about 315 °C by the existence of 0.3 wt% 3DGO. Compared to neat epoxy, the T_d of composite have increased about 35 °C, and with the increasing of the 3DGO loading, the T_d of composite and the char yields at 500 °C of 3DGO/epoxy gradually improved. Moreover, the maximum degradation temperature (T_{max}) of composite is apparently improved by the adding of GO from the DTG curves in Figure 5(b). It is a remarkable fact that the maximum of derivative weight of the materials is higher than neat epoxy resin with the trace amounts of 3DGO, and the maximum increase slowly along with the improvement of the dosage of 3DGO. This is mainly attributed to the three-dimensional network structure and heredity of GO. On the one hand, the thermal conductivity and stability of 3DGO is higher than epoxy matrix. On the other hand, three-dimensional network structure of GO provide pathways for the dispersion of heat, thus the decomposition of the materials was postponed to a large extent.

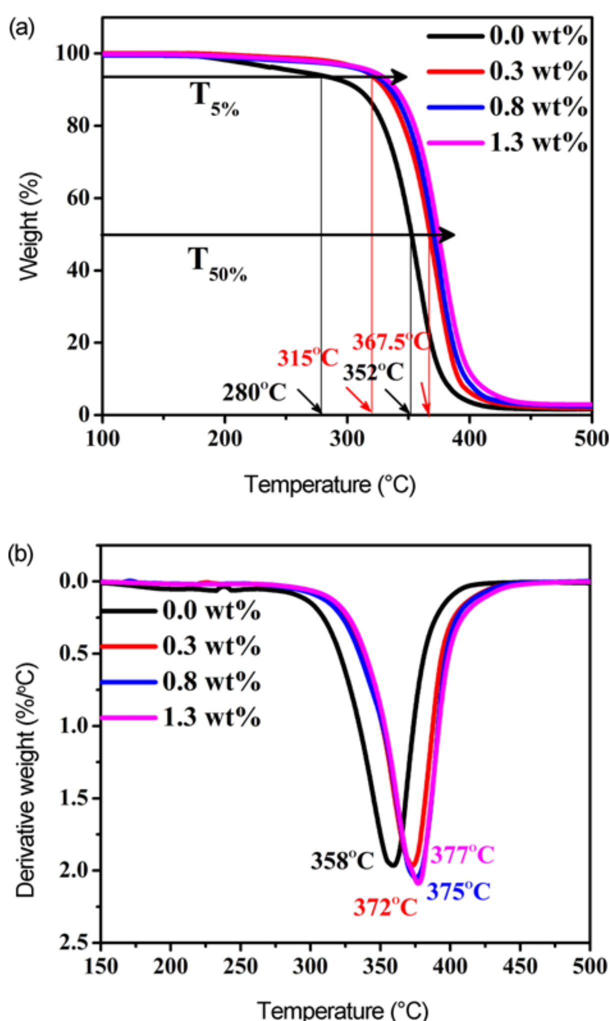

Figure 5. (a) TGA and (b) DTG curves of the neat epoxy and its composites.

Storage modulus and the glass transition temperature (T_g) as a vital indicator to evaluate the temperature dependent properties of materials were obtained by Dynamic mechanical analysis. As shown in Figure 6(a), the storage modulus of the materials was significantly improved with the existence of 3DGO in epoxy matrix. When the content of 3DGO reached 1.3 wt%, the epoxy materials achieved a higher storage modulus about 2600 MPa at 50 °C, which increase by 375 MPa compared to the 2235 MPa of neat epoxy. In addition, the storage modulus of epoxy composites increases with the increasing of the 3DGO loading. The T_g values were calculated from the maxima (peak) of tanδ curves shown in Figure 6(b). The T_g of neat epoxy polymer was about 187.5 °C, Whereas the T_g values of epoxy composite within the 3DGO were higher than neat epoxy. When the content of the 3DGO reached 0.3 wt%, the T_g of the epoxy composite was increased with the increasing the 3DGO loading. The main reason is that the joining of the 3DGO provided extra physical entanglements for epoxy matrix which ulteriorly restricted the movement of fragment of epoxy matrix in the course of heating. Moreover, 3DGO absorbed some of the energy and lead to delay of the glass-transition. Figure 6(c) and Figure 6(d) showed the storage modulus and tanδ curves of 1.3 wt% 3DGO/epoxy at the frequency of 0.5, 1, 5, 10, and 15 H_Z. Apparently, the storage modulus of composite improved slowly along with the increasing of the frequency and the maxima (peak) of tanδ curves moves toward the direction of higher frequency, suggesting that the storage modulus and the glass-transition of epoxy composite suffers from the dependence on the selection of different frequencies.

The thermal conductivity of epoxy composites with 3DGO is presented in Figure 7. It is evident that the thermal conductivity of epoxy composites increases steadily with the increasing of the 3DGO content. Meanwhile, the thermal diffusivity of the epoxy composites shows almost the similar change trend. But it is worth mentioning that the thermal conductivity of epoxy composite with only 0.3 wt% GO shows a remarkable improvement compared to the thermal conductivity of neat epoxy. The main reason for the phenomenon is the continuous three-dimensional network structure of GO in epoxy composites which provides the requisite pathway for heat conduction [40,41], but there is no this kind of structure in neat epoxy. By contrast, with the improvement of content of GO, the cross linking density of three-dimensional network structure gradually increases, which provides more pathways for heat conduction, therefore, the thermal conductivity increases relatively slowly. When the weight percentage of 3DGO is 1.3 wt%, the thermal

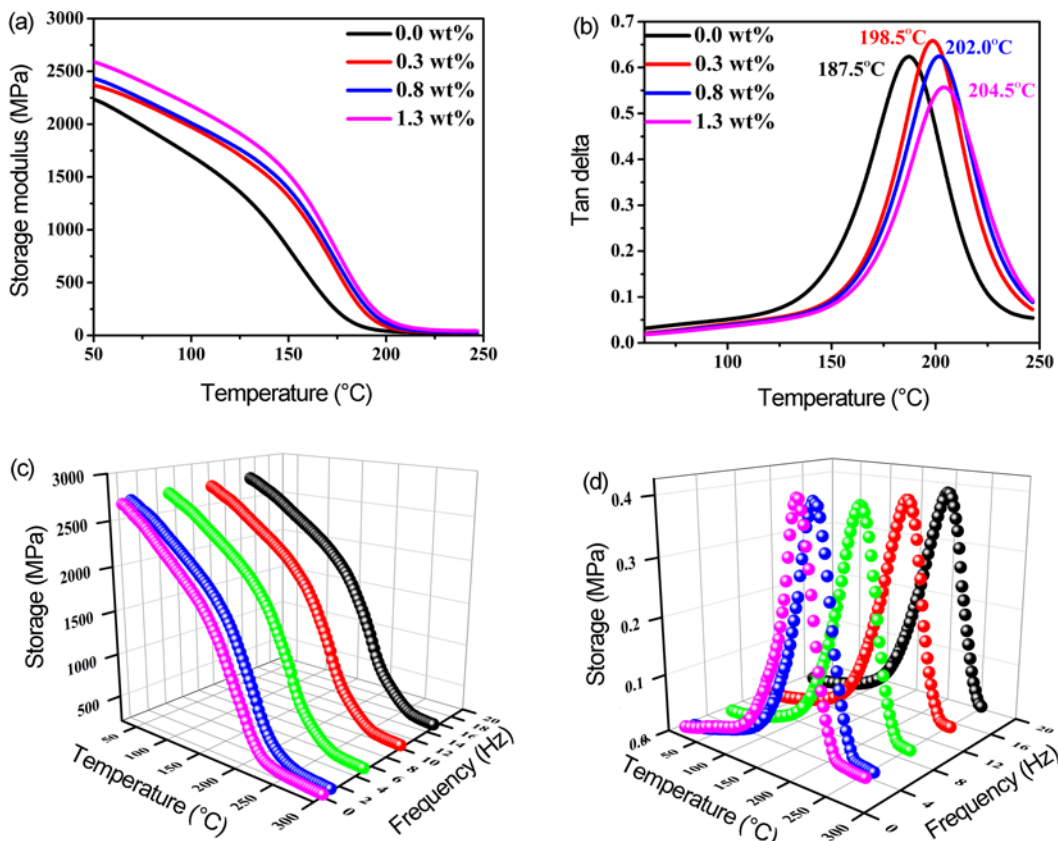

Figure 6. (a) Storage modulus of the neat epoxy and its composites in 1 H_Z, (b) Tanδ of the neat epoxy and its composites in 1 H_Z, (c) storage modulus of 1.3 wt% 3DGO/epoxy composite in different frequency, and (d) Tanδ of 1.3 wt% 3DGO/epoxy composite in different frequency.

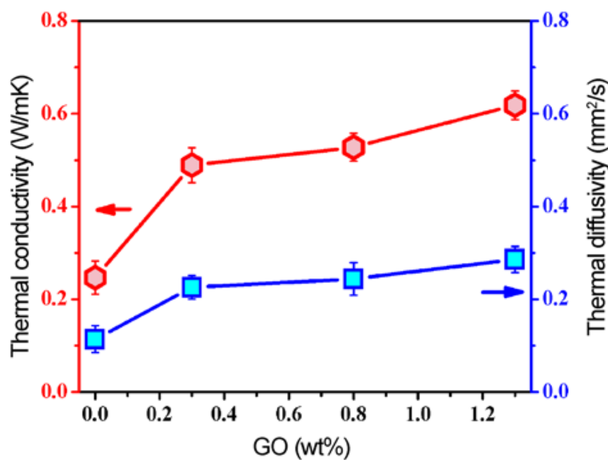

Figure 7. Thermal conductivity and thermal diffusivity of the neat epoxy and epoxy composites.

conductivity is 0.62 $Wm^{-1}K^{-1}$, increased by 148 % in comparison with that of the neat epoxy (0.25 $Wm^{-1}K^{-1}$). Table 1 summarizes the thermal conductivity of epoxy-based graphene composites reported in literature and the present research. One can see that the thermal conductivity enhancement value of our composites is higher than that of epoxy-based composites with the different type graphene fillers in previous works [42-47]. These reported composites have the interruption of heat flow between graphene fillers, there is a high thermal interface resistance and suppression of percolation. The three dimension structure of graphene oxide existed in this work, along with low thermal resistance between graphene filler, leading to high thermal conductivity for the composites.

Table 1. A comparison of various graphene filler for epoxy composites

Polymer matrix	Type of filler	Filler content (wt%)	Thermal conductivity enhancement (%)	Reference
Epoxy	Functionalized graphene	2.0	36	[42]
Epoxy	Functionalized graphene	3.0	90	[43]
Epoxy	Functionalized graphene	2.0	103	[44]
Epoxy	expanded graphite	1.5	50	[45]
Epoxy	Functionalized graphene	5.0	115	[46]
Epoxy	Functionalized graphene	0.5	103	[47]
Epoxy	Graphene oxide	1.3	148	This work

To demonstrate the effect on thermal performance of epoxy composites with 3DGO, results from a thermal image study are presented in Figure 8. The temperature profile evolution in time of two samples was captured using a calibrated infrared camera as the samples were heated from one side, as shown in Figure 8(a). Figure 8(b) shows that the surface temperature of two samples is almost exactly the same temperature. The main reason for that is the transfer of heat is not passed two sides of the samples in a very short period of time. By contrast, with the prolongation of heating time, the temperature in surface of epoxy composites with 1.3 wt% 3DGO is significantly higher than that of neat epoxy, as showed in Figure 8(c-e). The remarkable enhancement behavior is attributed that the 3DGO network play an important role for bridging the thermal conductive path between two sides in epoxy composites, and thus the thermal diffusivity and thermal conductivity of epoxy composites increase with increase of content of 3DGO.

A thermal expansion coefficient (TEC) is an important property of material, which is connected with the normal operation of electron component under a higher temperature [6]. Figure 9(a) shows the relationship between the change in the sample's length (ΔL) and temperature (T) of neat epoxy and epoxy composites before the T_g of neat epoxy. According to the well known formula

$$a(T) = \left(\frac{\Delta L}{L}\right)\left(\frac{1}{\Delta T}\right) \tag{1}$$

where $a(T)$ is the linear coefficient of thermal expansion, L is the original length of sample, ΔL is the change length of sample and $\Delta T = T - T_0$ (T is the actual temperature of sample and T_0 is the room temperature) [42]. The relationship between $a(T)$ and ΔT shown in Figure 9(b). Apparently, the value of ΔL of epoxy composites is lower than that of pure epoxy resin at the same temperature, and the values greatly decrease with the increasing of content of 3DGO, suggesting that the thermal stability of epoxy composites have enhanced by using of 3DGO. The $a(T)$ of epoxy composites containing 0.8 wt% and 1.3 wt% 3DGO always keep a lower growth rate, particularly the epoxy composite with 1.3 wt% 3DGO. Overall, however, the $a(T)$ of epoxy composite is lower than that of neat epoxy. The reason is the two factors as follows:

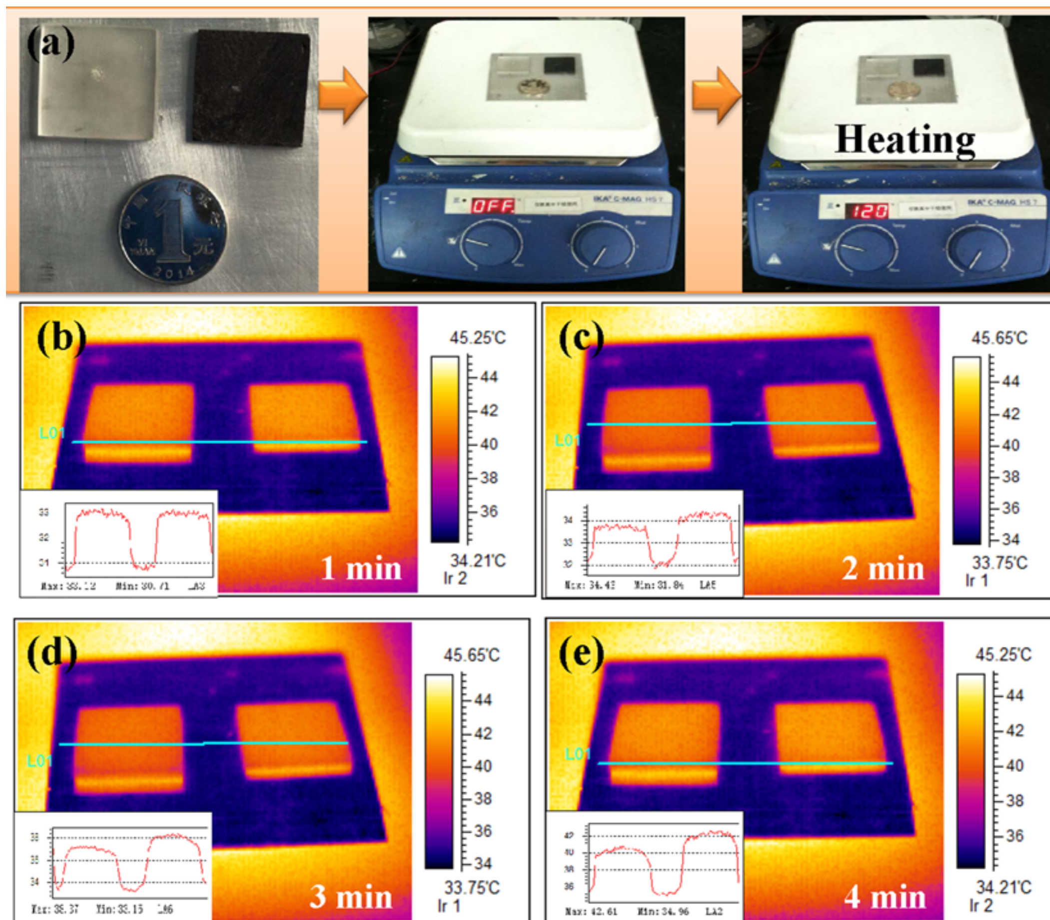

Figure 8. (a) Photograph of the neat epoxy and epoxy composite with 1.3 wt% 3DGO, (b-e) the thermogram of neat epoxy and epoxy composites with 1.3 % GO at different time.

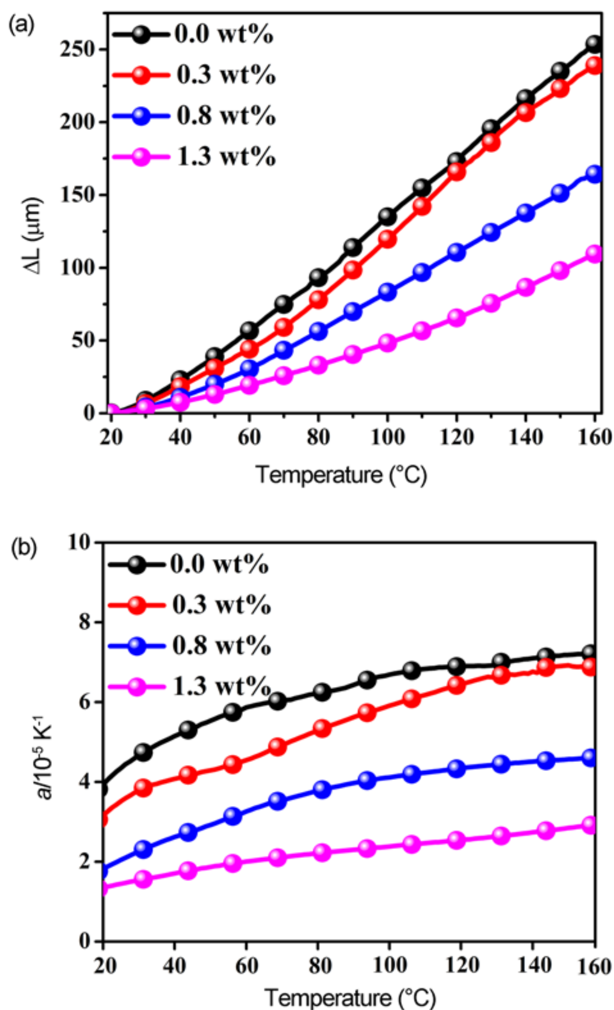

Figure 9. (a) The relationship between ΔL and T of the neat epoxy and its composites and (b) the relationship between a and T of the neat epoxy and its composites.

One is that GO has a poor thermal expansion and GO occupied the space between the molecules and narrowed the range of the small molecules, the group and chain segments. Another factor is that the special three-dimensional network of GO limited the expansion of epoxy matrix.

Conclusion

In summary, 3DGO/epoxy composites were successfully prepared by means of simple curing procedure. The 3DGO/epoxy exhibited synchronously relatively low thermal expansion properties and good thermal stability. Furthermore, the thermal conductivity of epoxy composites with only 1.3 wt% 3DGO is 0.62 $Wm^{-1}K^{-1}$, increased by 148 % in comparison with that of the neat epoxy (0.25 $Wm^{-1}K^{-1}$). In addition, the storage modulus of epoxy composite with 1.3 wt% GO was improved to 2600 MPa from the 2235 MPa of neat epoxy, and the glass-transition temperatures of 3DGO/epoxy is also remarkably improved. Therefore, the three dimensional graphene nanofillers show significant potential as novel and effective additives for next generation electronic devices.

Acknowledgements

The authors gratefully acknowledge the financial support by National Natural Science Foundation of China (51303034, 51573201, 51163004, 51463007, 51403124 and 51367007), the Natural Science Foundation of Guangxi Province, China (2013GXNSFAA019308, 2014GXNSFDA118006 and 2014GXNSFBA118034), Guangxi Universities Scientific Research Project (No.YB2014165), Natural Science Foundation of Ningbo (No.Y40307DB05), International Science and Technology Cooperation Program of Ningbo (No.2015D10003).

References

1. S. Waśkiewicz, K. Zenkner, E. Langer, M. Lenartowicz, and I. Gajlewicz, *Prog. Org. Coat*., **76**, 1040 (2013).
2. A. Gergely, I. Bertóti, T. Török, É. Pfeifer, and E. Kálmán, *Prog. Org. Coat*., **76**, 17 (2013).
3. Y. Hao, F. Liu, and E. H. Han, *Prog. Org. Coat*., **76**, 571 (2013).
4. B. G. Soares, M. L. Celestino, M. Magioli, V. X. Moreira, and D. Khastgir, *Synth. Met*., **160**, 1981 (2010).
5. A. A. Azeez, K. Y. Rhee, S. J. Park, and D. Hui, *Compos. Pt. B-Eng.*, **45**, 308 (2013).
6. Y. Luo, Y. Huang, X. Ren, X. Duan, and Q. Wang, *Opt. Commun*., **310**, 187 (2014).
7. B. Dercks, R. Zecirovic, G. Ruffert, M. P. Grün, and M. Grünewald, *Chemie Ingenieur Technik*, **83**, 1125 (2011).
8. R. J. McGlen, R. Jachuck, and S. Lin, *Appl. Therm. Eng*., **24**, 1143 (2004).
9. J. Felba, "Thermally Conductive Nanocomposites", pp.277-314, Nano-Bio-Electronic, Photonic and MEMS Packaging, Springer, 2010.
10. Y. X. Fu, Z. X. He, D. C. Mo, and S. S. Lu, *Int. J. Therm. Sci*., **86**, 276 (2014).
11. M. Lee, Y. Choi, K. Sugio, K. Matsugi, and G. Sasaki, *Compos. Sci. Technol*., **97**, 1 (2014).
12. J. Kováčik, Š. Emmer, and J. Bielek, *Int. J. Therm. Sci*., **90**, 298 (2015).
13. J. R. Choi, Y. S. Lee, and S. J. Park, *J. Ind. Eng. Chem.*, **20**, 3421 (2014).
14. H. Ji, S. Wang, M. Li, and J. Kim, *Mater. Lett*., **116**, 219 (2014).
15. J. Yu, X. Huang, L. Wang, P. Peng, C. Wu, X. Wu, and P. Jiang, *Polym. Chem*., **2**, 1380 (2011).
16. J. Yu, H. Mo, and P. Jiang, *Polym. Adv. Technol*., **26**, 514 (2015).
17. Y. Yao, X. Zeng, K. Guo, R. Sun, and J. B. Xu, *Compos. Pt. A-Appl. Sci. Manuf.*, **69**, 49 (2015).

18. G. Chen, W. Yang, R. Dong, M. Hussain, and G. Wu, *Mater. Des*., **63**, 109 (2014).
19. M. Farbod, A. Ahangarpour, and S. G. Etemad, *Particuology*, **22**, 59 (2015).
20. S. I. Kundalwal, R. Suresh Kumar, and M. C. Ray, *Int. J. Heat Mass Transfer*, **72**, 440 (2014).
21. Z. Hajjar, A. M. Rashidi, and A. Ghozatloo, *Int. Commun. Heat Mass Transfer*, **57**, 128 (2014).
22. X. Shen, X. Lin, J. Jia, Z. Wang, Z. Li, and J. K. Kim, *Carbon*, **80**, 235 (2014).
23. P. Kim, L. Shi, A. Majumdar, and P. L. McEuen, *Phys. Rev. Lett*., **87**, 215502 (2001).
24. A. A. Balandin, S. Ghosh, W. Bao, I. Calizo, D. Teweldebrhan, F. Miao, and C. N. Lau, *Nano Lett*., **8**, 902 (2008) .
25. Y. Wang, J. Yu, W. Dai, Y. Song, D. Wang, L. Zeng, and N. Jiang, *Polym. Compos*., **36**, 556 (2015) .
26. W. Dai, J. Yu, Y. Wang, Y. Song, H. Bai, K. Nishimura, H. Liao, and N. Jiang, *Macromol. Res*., **22**, 983 (2014).
27. J. T. Choi, D. H. Kim, K. S. Ryu, H. I. Lee, H. M. Jeong, C. M. Shin, J. H. Kim, and B. K. Kim, *Macromol. Res*., **19**, 809 (2011).
28. J. Guerrero-Contreras and F. Caballero-Briones, *Mater. Chem. Phys*., **153**, 209 (2015) .
29. J. Chen, B. Yao, C. Li, and G. Shi, *Carbon*, **64**, 225 (2013).
30. T. T. Wu and J. M. Ting, *Surf. Coat. Technol*., **231**, 487 (2013).
31. L. Sun and B. Fugetsu, *Mater. Lett*., **109**, 207 (2013).
32. J. Kim, M. Park, H. K. Shin, J. Choi, B. Pant, P. S. Saud, T. An, S. H. Chae, and H. Y. Kim, *Mater. Lett*., **149**, 15 (2015).
33. X. She, T. Liu, N. Wu, X. Xu, J. Li, D. Yang, and R. Frost, *Mater. Chem. Phys*., **143**, 240 (2013).
34. L. G. Cancado, A. Jorio, E. H. Ferreira, F. Stavale, C. A. Achete, R. B. Capaz, M. V. Moutinho, A. Lombardo, T. S. Kulmala, and A. C. Ferrari, *Nano Lett*., **11**, 3190 (2011).
35. J. Choi, N. D. K. Tu, S. S. Lee, H. Lee, J. S. Kim, and H. Kim, *Macromol. Res*., **22**, 1104 (2014) .
36. B. Tang, G. Hu, H. Gao, and L. Hai, *Int. J. Heat Mass Transfer*, **85**, 420 (2015).
37. C. Li and G. Shi, *Nanoscale*, **4**, 5549 (2012).
38. X. Wang, W. Xing, P. Zhang, L. Song, H. Yang, and Y. Hu, *Compos. Sci. Technol*., **72**, 737 (2012).
39. B. Ahmadi-Moghadam, M. Sharafimasooleh, S. Shadlou, and F. Taheri, *Mater. Des*., **66**, 142 (2015).
40. G. D. Park, H. O. Jung, K. M. Kim, J. H. Lim, J. W. Lee, S. G. Lee, J. H. Lee, and S. R. Kim, *Macromol. Res*., **23**, 396 (2015).
41. Y. X. Fu, Z. X. He, D. C. Mo, and S. S. Lu, *Appl. Therm. Eng*., **66**, 493 (2014).
42. S. Chatterjee, J. W. Wang, W. S. Kuo, N. H. Tai, C. Salzmann, W. L. Li, R. Hollertz, F. A. Nüesch, and B. T. T. Chu, *Chem. Phys. Lett*., **531**, 6 (2012).
43. J. Kim, B.-S. Yim, J.-M. Kim, and J. Kim, *Microelectron. Reliability*, **52**, 595 (2012).
44. T. Zhou, *Express Polym. Lett*., **9**, 608 (2015).
45. Z. Wang, R. Qi, J. Wang, and S. Qi, *Ceram. Int*., **41**, 13541 (2015).
46. F. Wang, L. T. Drzal, Y. Qin, and Z. Huang, *J. Mater. Sci*., **50**, 1082 (2014).
47. H. Ribeiro, W. M. da Silva, J. C. Neves, H. D. R. Calado, R. Paniago, L. M. Seara, D. D. Mercês Camarano, and G. G. Silva, *Polym. Test*., **43**, 182 (2015).
48. M. M. El-Tonsy, *Polym. Test*., **23**, 355 (2004).